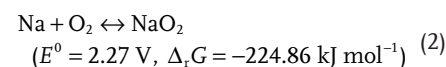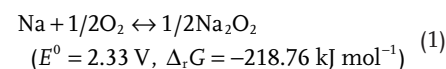# Sodium Peroxide Dihydrate or Sodium Superoxide: The Importance of the Cell Configuration for Sodium–Oxygen Batteries

Xuanxuan Bi, Rongyue Wang, Lu Ma, Dongzhou Zhang, Khalil Amine,* and Jun Lu*

In sodium–oxygen (Na–O$_2$) batteries, multiple discharge products have been observed by different research groups. Given the fact that different materials, gas supplies, and cell configurations are used by different groups, it is a great challenge to draw a clear conclusion on the formation of the different products. Here, two different cell setups are used to investigate the cell chemistries of Na–O$_2$ batteries. With the same materials and gas supplies, a peroxide-based product is observed in a glass chamber cell and a superoxide-based product is observed in a stainless-steel cell. Ex situ high-energy X-ray diffraction (HEXRD) and Raman spectroscopy are performed to investigate the structure and composition of the product. In addition, in situ XRD is used to investigate the structure evolution of the peroxide-based product. The findings highlight the importance of the cell design and emphasize the critical environment of the formation of the discharge products of Na–O$_2$ batteries.

1. Introduction

Recently, metal–air batteries have received great research interest due to their high theoretical energy densities, which could enable applications in electric vehicles or large energy-storage systems.[1] In a typical lithium–oxygen (Li–O$_2$) cell, the overall reaction follows: $2Li + O_2 \leftrightarrow Li_2O_2$, ($E^0 = 2.96$ V), where lithium peroxide is generally observed as the discharge product.[1b] In sodium–oxygen (Na–O$_2$) cells, different discharge products have been observed by different research groups. Two possible products, sodium peroxide (Na$_2$O$_2$) (sometimes in the form of Na$_2$O$_2$·2H$_2$O)[2] and sodium superoxide (NaO$_2$),[3] have been detected. The overall reactions are shown in Equation (1) and (2). The similar free energies of the two reactions imply that it is difficult to determine which product is more thermodynamically favorable.

$$Na + 1/2O_2 \leftrightarrow 1/2Na_2O_2$$
$$(E^0 = 2.33 \text{ V}, \Delta_rG = -218.76 \text{ kJ mol}^{-1}) \quad (1)$$

$$Na + O_2 \leftrightarrow NaO_2$$
$$(E^0 = 2.27 \text{ V}, \Delta_rG = -224.86 \text{ kJ mol}^{-1}) \quad (2)$$

The various discharge products originate from the different cell chemistries of Na–O$_2$ batteries. The intrinsic properties such as the crystal structure and electron/ionic conductivity of sodium peroxide and sodium superoxide greatly affect the kinetics in the cells, resulting in different electrochemical behaviors at the oxygen-evolution-reaction (OER) process.[4] Most studies with Na$_2$O$_2$ or Na$_2$O$_2$·2H$_2$O as the product have showed sluggish kinetics during the OER and a charge over-potential over 1 V was observed on a bare carbon cathode.[5] Multiple OER catalysts have been investigated to reduce the charging polarization, which is similar to the scenario in Li–O$_2$ batteries.[6] In contrast to peroxides-based Na–O$_2$ batteries, Hartmann et al. discovered NaO$_2$ as the major discharge product in their Na–O$_2$ batteries, resulting in a charge overpotential as low as 0.2 V.[1c] Based on the discrepancies on the discharge products, Bender et al. reviewed most studies in the field of Na–O$_2$ and pointed out that detailed information of the cell configuration was missing, leading to confusion of the formation of the different discharge products.[7]

Here, we investigate the cell chemistries of Na–O$_2$ batteries using two different cell setups with exactly the same sodium anode, glass-fiber separator, carbon-paper cathode, electrolyte, and oxygen-gas supply system. Our study reveals that in a stainless-steel cell, the superoxide-based product is observed as the only discharge product, while in a glass chamber cell, the peroxide-based product was the only discharge product. Based on the formation of peroxide, in situ XRD was carried out to investigate the discharge/charge process to understand the cell chemistry in the glass chamber cell. Our results indicate that

X. Bi, Dr. K. Amine, Dr. J. Lu
Chemical Sciences and Engineering Division
Argonne National Laboratory
9700 South Cass Avenue, Lemont, IL 60439, USA
E-mail: amine@anl.gov; junlu@anl.gov
X. Bi
Department of Chemistry and Biochemistry
The Ohio State University
100 West 18th Avenue, Columbus, OH 43210, USA
Dr. R. Wang
Energy Systems Division
Argonne National Laboratory
9700 South Cass Avenue, Lemont, IL 60439, USA
Dr. L. Ma
X-ray Science Division
Argonne National Laboratory
9700 South Cass Avenue, Lemont, IL 60439, USA
Dr. D. Zhang
HIGP
University of Hawaii at Manoa
1680 East-West Rd, Honolulu, HI 96822, USA

The ORCID identification number(s) for the author(s) of this article can be found under https://doi.org/10.1002/smtd.201700102.
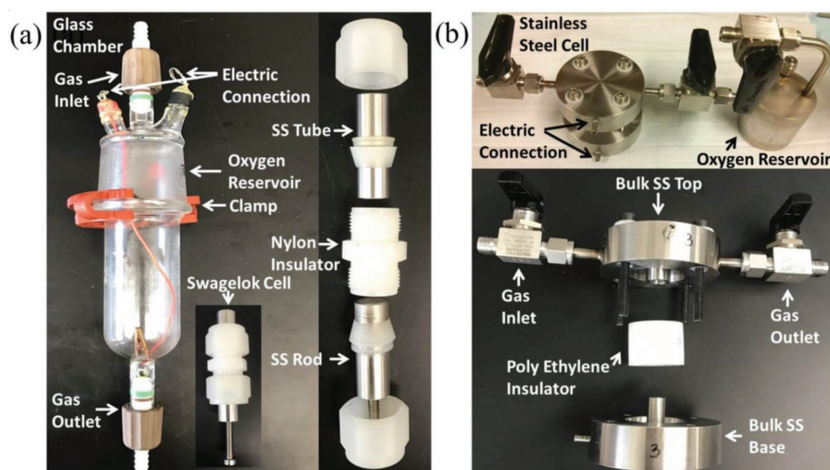
Figure 1. a,b) Optical images of the Swagelok cell sealed in a glass chamber (GC) (a), and the stainless-steel (SS) cell sealed by two bulk stainless-steel pieces and a polyethylene holder (b).

the formation of the discharge products in Na–O$_2$ batteries greatly relies on the type of sealing of the cell. The formation of NaO$_2$ is guaranteed in a well-sealed, pressure-tolerant device, while a small amount of air leakage will lead to peroxide formation. The work provides insights to understand the electrochemical process in peroxide-based Na–O$_2$ cells and brings up the importance of the cell design for Na–O$_2$ batteries.

2. Results and Discussions

The optical images of the two different setups are shown in **Figure 1**. The glass-chamber cell setup, shown in Figure 1a, use a Swagelok cell containing a 1/2 in. (outer diameter, O.D.) stainless-steel rod and a 1/2 in. (O.D.) stainless-steel tube tightly scrolled by the Swagelok nylon parts. The stainless-steel rod serves as the current collector for the metal anode, while the tube is open to the oxygen allowing gas diffusion through the air electrode. A stainless-steel mesh is used as the support material and current collector for the air electrode. After the cell is assembled, it is placed in a home-made glass chamber (GC), which serves as the oxygen reservoir with two adjustable valves for gas flow. Two clips wiring out of the chamber are the electric connections to the electrochemical testing station. The top piece and the bottom piece of the glass chamber are sealed by high-vacuum grease and then tightened by a large snap ring.

The stainless-steel cell setup (SS) is shown in Figure 1b. The bulk stainless-steel base and top pieces are sealed by two O-rings on both sides of a polyethylene holder (inner diameter: 1/2 in.), isolating the cell from air. The rod in the center of the stainless-steel base is the support for the sodium anode. A stainless-steel mesh, the same as that in the GC cell, is used as the current collector for the cathode and a stainless-steel spring washer is used as a buffer to the pressure from the top piece of the stainless-steel cell.

A stainless-steel oxygen reservoir is attached to the cell for oxygen storage.

The two cell setups share similarities but there are differences between the cell configurations. For the similarities, all the materials including the sodium metal, glass-fiber separators, carbon-paper cathodes, and the electrolytes were completely identical and prepared at the same time. For both cells, the diameter of the separator was 1/2 in., and the diameter of the carbon electrode was 7/16 in. converting to a surface area of 1 cm^2. The current was 0.1 mA for all galvanostatic tests in this study, which was equivalent to a current density of 0.1 mA cm^{-2}. Furthermore, the same gas-supply line connected by high-pressure poly(vinyl chloride) (PVC) clear tubing was applied for oxygen flow, and both cells used static oxygen stored in the oxygen reservoir. In addition, for comparison, the two cells were assembled simultaneously and the electrodes were characterized after the same duration. Nevertheless, differences exist in the two cells based on the different cell configurations. The GC cell used glass as the material of the oxygen reservoir and vacuum grease for the sealing, whereas the SS cell used a stainless-steel oxygen reservoir and O-rings for the sealing material. The different sealing method might allow air leakage into the system and result in different cell chemistries. Other parameters such as oxygen partial pressure, oxygen flow time, and water content in the electrolyte were also investigated in this study but these factors were not able to change the cell chemistry (shown in the following section).

The first discharge/charge profiles of the Na–O$_2$ batteries based on the two cell setups are shown in **Figure 2**. The voltage window is set from 1.8 to 4.0 V. For the GC cell (Figure 2a), the discharging voltage shows a steady plateau at 2.16 V, whereas the charging process displays three plateaus, at 2.5, 3.4, and 3.6 V, respectively. The high charging voltage indicates the formation of peroxide-based products, consistent with previous studies.[2a,5] Nevertheless, in the SS cell, the discharge/charge profile is more reversible. The discharge voltage is 2.09 V and it is slightly lower than that in the GC cell. Moreover, the charging plateau stays at 2.31 V followed by a dramatic increase up to the limiting voltage of 4.0 V.[3a,8] The low charging voltage
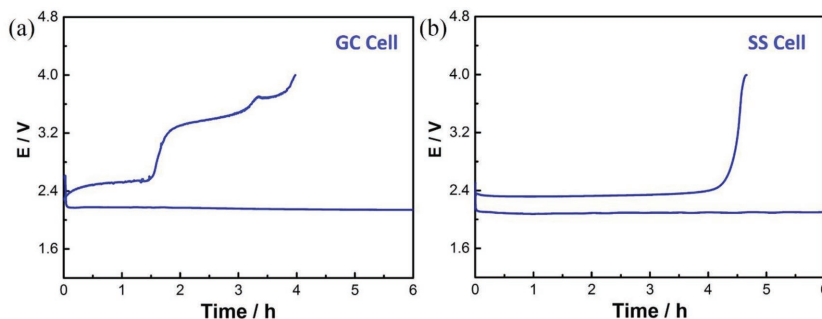

Figure 2. a,b) Discharge/charge profiles of Na–O$_2$ cells in a glass chamber (GC) cell (a) and a stainless-steel (SS) cell (b). The current density is 1 mA cm^{-2}.
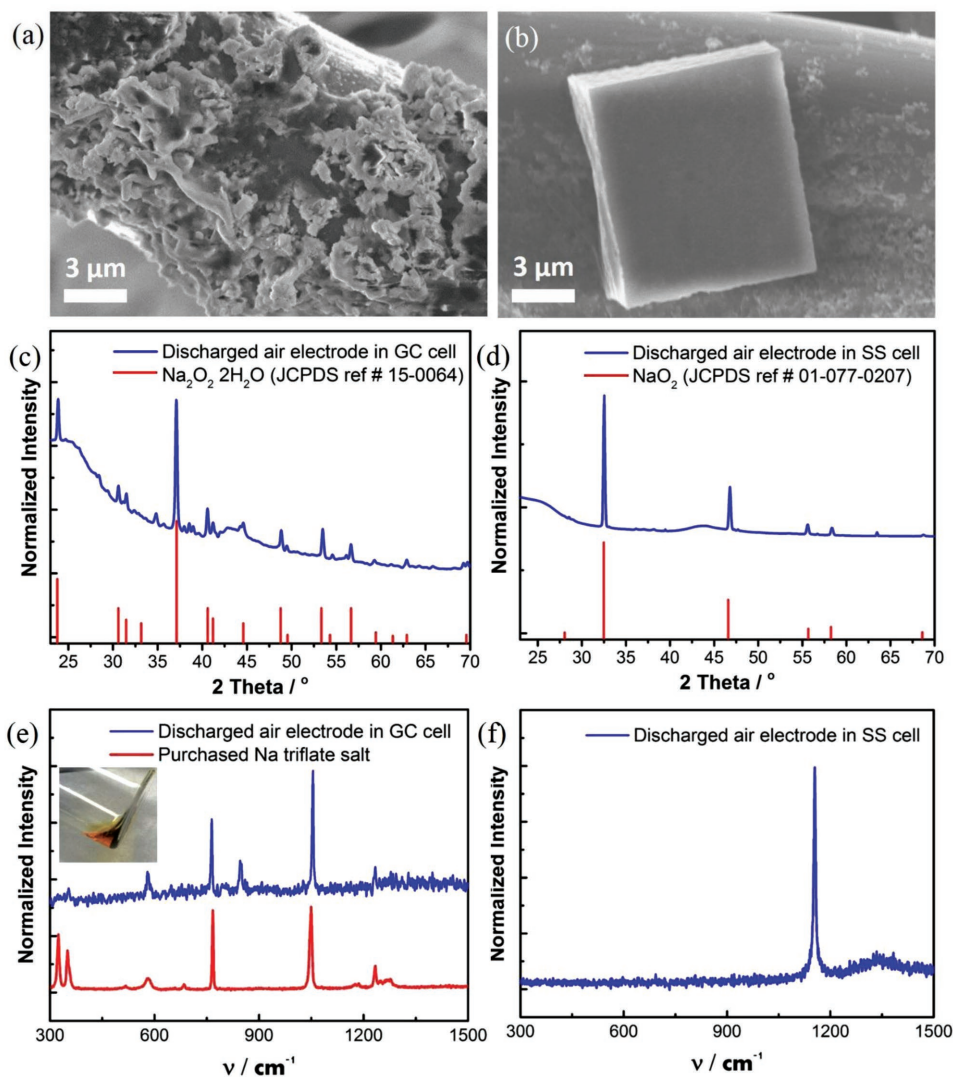
Figure 3. a,c,e) SEM images (a), HE-XRD (c), and Raman spectra (e) of the discharge product in GC cell. b,d,f) SEM images (b), high-energy XRD (HE-XRD) (d), and Raman spectra (f) of the discharge product in SS cell.

shows that the decomposition of the discharge product only contributes little overpotential to the charging process, which is a result from a kinetically favorable process.[9] The voltage increase at the end of charge implies the depletion of the rechargeable product.

When the GC cell and the SS cell were discharged for 10 h, they were disassembled and the air-diffusion layers were characterized by scanning electron microscopy (SEM), high-energy X-ray diffraction (HE-XRD), and Raman spectroscopy. For the SEM measurements, the samples were protected in a Mason jar under an Ar atmosphere during the transfer to the chamber. **Figure 3**a shows the morphology of the discharge product in the GC cell. It has an irregular shape with a rod-like structure and unevenly disperses on the surface of carbon fibers, which is very different from the sodium peroxide dihydrate ($Na_2O_2 \cdot 2H_2O$) reported in previous studies.[2b,4b] In contrast, the discharge product in the SS cell displays a typical cubic structure with a sharp edge (Figure 3b), indicating the formation of NaO_2. The size of the cube is around 7–10 µm.

Interestingly, although the two cells use the same materials and electrolytes, the morphologies are completely different. To further identify the crystalline structure and the composition of the discharge products, HE-XRD and Raman spectroscopy were carried out. For HE-XRD, the discharged air diffusion layers were sealed by Kapton tapes and were tested in transmission mode. Figure 3c shows the XRD patterns of the discharge product (blue curve) formed in the GC cell and the standard patterns of $Na_2O_2 \cdot 2H_2O$ (red vertical lines) from the crystal-phase database (JCPDS reference card number 15-0064). The diffractions of the discharge product match well with the standard $Na_2O_2 \cdot 2H_2O$ and there is no superoxide detected. However, in the SS cell, the main discharge product is proved to be NaO_2 (Figure 3d), compared to the standard patterns obtained by JCPDS reference card number 01-077-0207. The Raman spectrum further proves that NaO_2 is the major discharge product due to the unique peak from superoxide species at 1156 cm^{-1} (Figure 3f).[1c] The broad peak at 1335 cm^{-1} is from the D-band of the carbon substrate.

Figure 3e shows the Raman spectrum of the discharged air diffusion layer in the GC cell and purchased Na triflate salt is used as the control material. From the Raman spectra, multiple peaks of the sodium salt are observed due to the precipitation from the electrolyte. Besides, we observe an additional peak at 860 cm^{-1} instead of standard signals from Na_2O_2 located at 735 and 791 cm^{-1}. The same experiments had been repeated multiple times and the peaks ranging from 860 to 864 cm^{-1} were observed each time. Ortiz-Vitoriano et al. and Kim et al. report that the vibration of $Na_2O_2 \cdot 2H_2O$ is located at 1136 cm^{-1} but the peak is not observed here.[3c,10] It should be noted that the formation of $Na_2O_2 \cdot 2H_2O$ in the previous studies was from the decomposition of NaO_2, while in our study $Na_2O_2 \cdot 2H_2O$ was directly formed at the beginning of the discharge. The different formation pathways might generate different forms of the products. In addition, Sayed et al. argue that the peak at 1141 cm^{-1} might come from the Na_2O_2 or the CH_3O and $C-O$ groups.[11] It is likely that during the aging of NaO_2, it reacts with the electrolyte to form side products. The signal at 860 cm^{-1} is most likely from hydrogen peroxide (H_2O_2) since Giguere and co-workers report that the stretch of $O-O$ bond in H_2O_2 is located at 865 cm^{-1}.[12] To further confirm the presence of peroxide in the discharge product, a titration method was performed using the titanium oxysulfate ($TiOSO_4$) aqueous solution, which is selective to both superoxide and peroxide-based compounds.[8b] After immersing the discharged air electrode in the solution, it changed color from transparent to dark yellow (inset in Figure 3e). Since there is no superoxide detected in the XRD and Raman spectroscopy measurements for the GC cell, the color change results from the peroxide species in the discharge product. Given that the detailed structural information of $Na_2O_2 \cdot 2H_2O$ is still missing to date[13] and the Raman spectra show the presence of H_2O_2 in the discharge product, we cautiously suggest that the structure of the peroxide-based product is $2NaOH \cdot H_2O_2$, which shares the same chemical formula as $Na_2O_2 \cdot 2H_2O$.

In order to understand the structural evolution of the peroxide-based product during discharge/charge of the Na–O$_2$ battery, in situ XRD was performed using high-energy X-rays at the Advanced Photon Source (APS), Argonne National Laboratory. The detailed experimental parameters are included in the Experimental Section. The in situ cell has a large oxygen reservoir similar to the glass chamber and two Kapton sealed windows for the transmission of X-rays. Moreover, a coin cell replaced the Swagelok cell to minimize the cell thickness. Small holes were prepunched in the middle of the coin-cell cases, washers, and sodium metal, and thus only the carbon electrode and glass-fiber separator soaked with electrolyte were exposed to X-rays. The voltage profiles of the in situ cell are shown in **Figure 4** corresponding to the XRD patterns during the discharge/charge process. The discharge shows one plateau at 2.17 V, while the charge process displays three plateaus. The red vertical lines at the top represent the standard patterns of peroxide-based product and the green lines at the
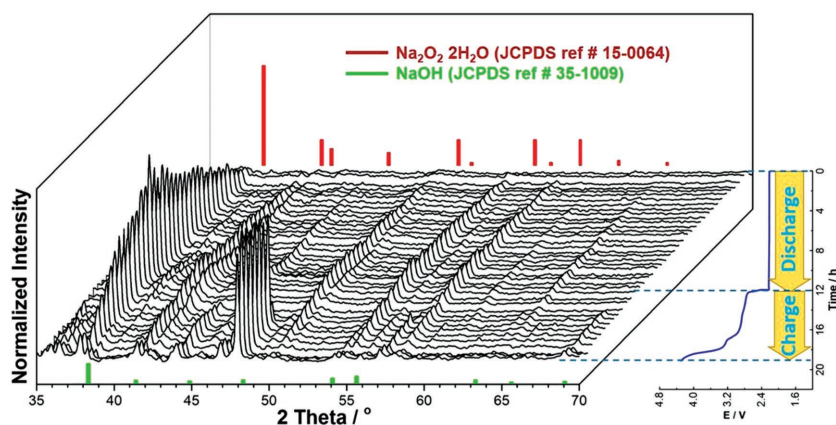

Figure 4. The in situ HE-XRD of the Na–O$_2$ battery tested in GC cell. From the top to the bottom, the cell first discharges and then charges. The current density is 0.1 mA cm^{-2}.

bottom are the standard patterns of sodium hydroxide (NaOH, JCPDS reference card number 35-1009). At the beginning of the discharge, the diffraction of peroxide-based product is observed and no NaO_2 is formed, confirming that it is the only discharge product detected in the XRD. With the increase of the depth of discharge, the peak intensity increases, indicating the accumulation of the discharge product. For the charging process, the first plateau at around 2.7 V corresponds to the decomposition of the peroxide-based product.[14] With the increase of the state of charge, the signals of NaOH at 38.3°, 54.0°, and 55.6° start to emerge at the end of the first plateau and keep increasing to the end of charge. At the second and the third plateaus, the decomposition of the peroxide-based discharge product continues, but a prominent signal at 48.0° is observed, which is very likely to be sodium carbonate (Na_2CO_3). The presence of additional peaks indicates that side products are formed during charge especially when the voltage exceeds 3.3 V. They might originate from the decomposition of the electrolyte. The formation of side products are probably the major obstacle for the low capacity retention of peroxide-based Na–O$_2$ batteries.

To investigate the influence of the side products formed at high charge voltage, the cyclability of Na–O$_2$ batteries in both the GC cell and the SS cell were explored (**Figure 5**). The GC cell only runs three cycles with a voltage window of 1.8–4.0 V and the round-trip efficiency is around 70% for each cycle, whereas in the SS cell, the cyclability reaches 80 cycles with over 90% round-trip efficiency using a voltage window of 1.8–3.6 V. It is worth noting that for the GC cell, although the round-trip efficiency is low, the in situ HE-XRD results suggest that almost all the peroxide-based product has been removed from the electrode. It is suggested that the reaction in the GC cell is irreversible.

The comparisons of the two cell configurations such as oxygen flow time, oxygen partial pressure, and water content in electrolyte are investigated, shown in **Table 1** (the XRD and Raman spectroscopy data are not listed here). However, those factors are not the major reasons for the formation of different discharge products. Pinedo et al. considered multiple factors such as current density, size effect, oxygen pressure, and gas moisture, and discovered that gas moisture is the key issue
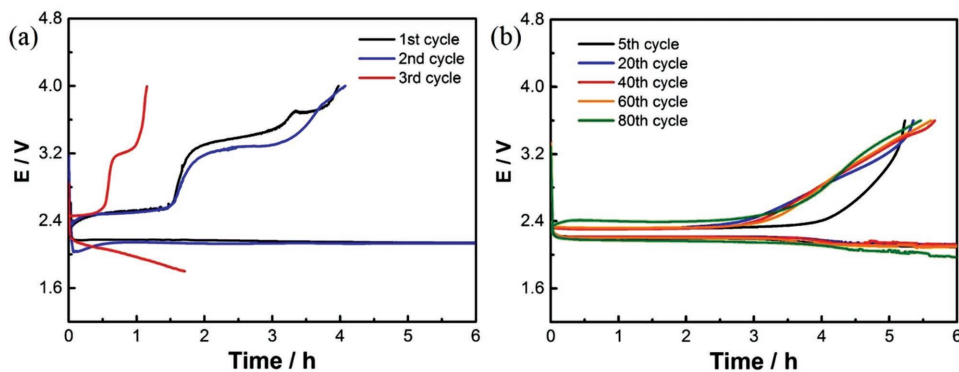
Figure 5. a,b) Cyclability tests in the GC cell (a) and the SS cell (b). The current density is 0.1 mA cm^{-2} for both the GC cell and the SS cell.

for the formation of $Na_2O_2 \cdot 2H_2O$, which was probably from the gas/water leakage.[15] Ortiz-Vitoriano et al. discovered that even when the water content is as high as 6000 ppm, NaO_2 is still the major discharge product except when exposing NaO_2 to air.[3c,16] It is very unlikely that the GC cell has a huge amount of water (≫6000 ppm) from the air before discharge but the peroxide-based product is observed at the beginning of the discharge. Nevertheless, the formation of the peroxide-based product requires water either from the air atmosphere or the decomposition of the solvent. In our study, the vacuum-grease-sealed glass chamber might cause air leakage. The impurities from the air could contribute to the formation of the peroxide-based product but the mechanism is not clear at this stage. More experiments and calculations are required in future work.

3. Conclusion

In conclusion, using two different cell setups in Na–O$_2$ batteries, different discharge products are observed. In the GC

cell the discharge product is a peroxide-based product, while in the SS cell it is a superoxide-based product, which are confirmed by HE-XRD and Raman spectroscopy. In situ HE-XRD for the GC cell shows that the single plateau during the discharge is only related to the formation of the superoxide-based product, while the three charge plateaus correspond to the decomposition of the peroxide-based product (2.7 V) and side reactions (>3.3 V). Our results reveal that the environment for the formation of NaO_2 is critical and that even a small portion of air leakage might lead to a completely different discharge product. This work could help to guide for the future application of superoxide-based Na–O$_2$ batteries especially for large-scale application.

4. Experimental Section

The Materials and Cell Assembly: A sodium metal slice (Fisher Scientific, labgrade) was used as the metal anode and H23 (Freudenberg) carbon paper was used as the air electrode. The electrolyte was bis (2-methoxyethyl) ether (diglyme, Sigma–Aldrich, 99.5%) containing 1 M sodium trifluoromethanesulfonate (sodium triflate, Sigma–Aldrich, 98%). The sodium triflate salt was dried in a vacuum oven at 120 °C overnight. Separators and carbon papers were dried in the vacuum oven at 100 °C for 20 h. The solvent was dried with 3 Å molecular sieves (Sigma–Aldrich) before use. The water content in the electrolyte was tested using a Mettler Toledo C20 Karl Fischer Coulometer. Two pieces of glass-fiber paper (Whatman, 300 µm thickness) were used as the separator. The gas supply is ultrahigh-purity oxygen gas (99.993%, UHP). The titration solution is diluted titanium(IV) oxysulfate (TiO(SO$_4$)) solution (≈2%, Sigma–Aldrich).

Before each battery performance test, oxygen gas was flowed into the sodium–oxygen battery and stored in the oxygen reservoir. All the cells were assembled in a glove box under high-purity argon (O$_2$ content < 0.1 ppm, H$_2$O content < 0.5 ppm) and stayed for 1 h to reach equilibrium before tests. The battery performance tests were performed using a Maccor testing station (model: 4000). The current density was set to 0.1 mA cm^{-2}.

Characterization Methods: Ex situ XRD was performed by HE-XRD with a wavelength of 0.117 418 Å at experimental station 11-ID-C of the APS, Argonne National Laboratory. In order to compare with the normal XRD, the wavelength was converted to 1.5418 Å (Cu K$_\alpha$), consistent with most studies. The samples were placed in a tiny holder (inner diameter: 3 mm) and sealed by Kapton tape on each side to avoid the contact to air.

In situ powdered XRD was carried out at the experimental station 13-BM-C at APS. The X-ray beam was monochromated with silicon 311

Table 1. The discharge products in the GC cell and SS cell based on multiple factors. The discharge products are confirmed by XRD and Raman spectroscopy.

Factors	Products	
	GC cell	SS cell
O$_2$ flow time		
1 min	Na$_2$O$_2$ 2H$_2$O	NaO$_2$
10 min	Na$_2$O$_2$ 2H$_2$O	NaO$_2$
30 min	Na$_2$O$_2$ 2H$_2$O	NaO$_2$
O$_2$ partial pressure		
0.5 atm (balance Ar)	Na$_2$O$_2$ 2H$_2$O	NaO$_2$
1 atm	Na$_2$O$_2$ 2H$_2$O	NaO$_2$
2 atm	Na$_2$O$_2$ 2H$_2$O	NaO$_2$
Water content in electrolyte		
≈20 ppm	Na$_2$O$_2$ 2H$_2$O	NaO$_2$
≈300 ppm	Na$_2$O$_2$ 2H$_2$O	NaO$_2$
≈4000 ppm	Na$_2$O$_2$ 2H$_2$O	NaO$_2$

crystal to 28.6 keV (0.434 Å), with a 1 eV bandwidth. A Kirkpatrick–Baez mirror system was used to obtain a vertical × horizontal focus spot size of 20 μm × 30 μm, measured as full width at half maximum (FWHM). The diffraction pattern was collected in a transmission way, and an MAR165 charge-coupled-device (CCD) detector (Rayonix) was placed about 170 mm away from the sample. LaB_6 powder was used to calibrate the distance and tilting of the detector. The typical exposure time for each diffraction pattern was 120 s. The diffraction patterns were integrated and analyzed by the DIOPTAS software (Prescher and Prakapenka, 2015). A home-made in situ XRD holder similar to the glass chamber cell was used in the test. The transmission X-ray went across two well-sealed Kapton tape windows on each side of the holder. A 2032 coin cell was assembled with the same materials and same electrolyte as above. During the XRD test, a Maccor (model: 4301) testing machine was used to gather the galvanostatic results in the meantime. The XRD data were collected at the same point every 30 min. After the measurements, the wavelength was converted to Cu K_α (1.5418 Å).

The battery products and surface-layer components on the air electrode were characterized by Raman spectrometer (inVia, Renishaw) with an excitation wavelength of 633 nm (laser power 6 mW). An airtight sample holder was made with an aluminum base with a quartz window and sealed by two O-rings.

SEM was performed using a Hitachi S4700 scanning electron microscope. Glass vials sealed in a Mason jar were used to store the samples before testing. The samples were quickly transferred from the Mason jar to the SEM sample chamber exposing to air within 10 s.

Conflict of Interest

The authors declare no conflict of interest.

[1] a) J. Lu, L. Li, J. B. Park, Y. K. Sun, F. Wu, K. Amine, *Chem. Rev.* **2014**, *114*, 5611; b) D. Aurbach, B. D. McCloskey, L. F. Nazar, P. G. Bruce, *Nat. Energy* **2016**, *1*, 16128; c) P. Hartmann, C. L. Bender, M. Vracar, A. K. Durr, A. Garsuch, J. Janek, P. Adelhelm, *Nat. Mater.* **2013**, *12*, 228; d) X. Ren, Y. Wu, *J. Am. Chem. Soc.* **2013**, *135*, 2923.

[2] a) Z. Jian, Y. Chen, F. Li, T. Zhang, C. Liu, H. Zhou, *J. Power Sources* **2014**, *251*, 466; b) H. Yadegari, M. N. Banis, B. Xiao, Q. Sun, X. Li, A. Lushington, B. Wang, R. Li, T.-K. Sham, X. Cui, X. Sun, *Chem. Mater.* **2015**, *27*, 3040; c) J. Lu, Y. J. Lee, X. Luo, K. C. Lau, M. Asadi, H.-H. Wang, S. Brombosz, J. Wen, D. Zhai, Z. Chen, D. J. Miller, Y. S. Jeong, J.-B. Park, Z. Z. Fang, B. Kumar, A. Salehi-Khojin, Y.-K. Sun, L. A. Curtiss, K. Amine, *Nature* **2016**, *529*, 377.

[3] a) P. Hartmann, D. Grübl, H. Sommer, J. Janek, W. G. Bessler, P. Adelhelm, *J. Phys. Chem. C* **2014**, *118*, 1461; b) C. Xia, R. Black, R. Fernandes, B. Adams, L. F. Nazar, *Nat. Chem.* **2015**, *7*, 496; c) N. Ortiz-Vitoriano, T. P. Batcho, D. G. Kwabi, B. Han, N. Pour, K. P. Yao, C. V. Thompson, Y. Shao-Horn, *J. Phys. Chem. Lett.* **2015**, *6*, 2636; d) I. Landa-Medrano, R. Pinedo, X. Bi, I. Ruiz de Larramendi, L. Lezama, J. Janek, K. Amine, J. Lu, T. Rojo, *ACS Appl. Mater. Interfaces* **2016**, *8*, 20120; e) X. Bi, X. Ren, Z. Huang, M. Yu, E. Kreidler, Y. Wu, *Chem. Commun.* **2015**, *51*, 7665.

[4] a) S. Yang, D. J. Siegel, *Chem. Mater.* **2015**, *27*, 3852; b) S. Kang, Y. Mo, S. P. Ong, G. Ceder, *Nano Lett.* **2014**, *14*, 1016.

[5] a) W. Liu, Q. Sun, Y. Yang, J. Y. Xie, Z. W. Fu, *Chem. Commun.* **2013**, *49*, 1951; b) Y. Li, H. Yadegari, X. Li, M. N. Banis, R. Li, X. Sun, *Chem. Commun.* **2013**, *49*, 11731.

[6] W.-M. Liu, W.-W. Yin, F. Ding, L. Sang, Z.-W. Fu, *Electrochem. Commun.* **2014**, *45*, 87.

[7] C. L. Bender, D. Schroder, R. Pinedo, P. Adelhelm, J. Janek, *Angew. Chem., Int. Ed.* **2016**, *55*, 4640.

[8] a) C. L. Bender, P. Hartmann, M. Vračar, P. Adelhelm, J. Janek, *Adv. Energy Mater.* **2014**, *4*, 1301863; b) P. Hartmann, C. L. Bender, J. Sann, A. K. Durr, M. Jansen, J. Janek, P. Adelhelm, *Phys. Chem. Chem. Phys.* **2013**, *15*, 11661.

[9] K. B. Knudsen, J. E. Nichols, T. Vegge, A. C. Luntz, B. D. McCloskey, J. Hjelm, *J. Phys. Chem. C* **2016**, *120*, 10799.

[10] J. Kim, H. Park, B. Lee, W. M. Seong, H. D. Lim, Y. Bae, H. Kim, W. K. Kim, K. H. Ryu, K. Kang, *Nat. Commun.* **2016**, *7*, 10670.

[11] S. Y. Sayed, K. P. Yao, D. G. Kwabi, T. P. Batcho, C. V. Amanchukwu, S. Feng, C. V. Thompson, Y. Shao-Horn, *Chem. Commun.* **2016**, *52*, 9691.

[12] a) P. A. Giguere, T. K. K. Srinivasan, *J. Raman Spectrosc.* **1974**, *2*, 152; b) S. Venkateswaran, *Nature* **1931**, *127*, 406; c) T. K. K. Srinivasan, P. A. Giguere, *Chem. Phys. Lett.* **1975**, *33*, 479.

[13] a) T. P. Firsova, A. N. Molodkina, T. G. Morozova, N. N. Stasevich, *Bull. Acad. Sci. USSR, Div. Chem. Sci.* **1966**, *15*, 724; b) N.-G. Vannerberg, in *Progress in Inorganic Chemistry*, Vol. 4, (Ed.: F. A. Cotton), John Wiley & Sons, **1962**, p. 164.

[14] H. Yadegari, Y. Li, M. N. Banis, X. Li, B. Wang, Q. Sun, R. Li, T.-K. Sham, X. Cui, X. Sun, *Energy Environ. Sci.* **2014**, *7*, 3747.

[15] R. Pinedo, D. A. Weber, B. Bergner, D. Schröder, P. Adelhelm, J. Janek, *J. Phys. Chem. C* **2016**, *120*, 8472.

[16] I. I. Abate, L. E. Thompson, H. C. Kim, N. B. Aetukuri, *J. Phys. Chem. Lett.* **2016**, *7*, 2164.